


RESEARCH ARTICLE

Cortical pattern of reduced perfusion in hearing loss revealed by ASL-MRI

Sara Ponticorvo¹ | Renzo Manara¹ | Josef Pfeuffer² | Arianna Cappiello³ | Sofia Cuoco³ | Maria Teresa Pellecchia^{1,3} | Renato Saponiero⁴ | Donato Troisi^{1,3} | Claudia Cassandro³ | Marta John¹ | Alfonso Scarpa³ | Ettore Cassandro^{1,3} | Francesco Di Salle^{1,4} | Fabrizio Esposito^{1,4} 

¹Department of Medicine, Surgery and Dentistry, Scuola Medica Salernitana, University of Salerno, Salerno, Italy

²MR Application Development, Siemens Healthcare GmbH, Erlangen, Germany

³Department of Neurosciences and Craniofacial Disorders, Scuola Medica Salernitana, University Hospital "San Giovanni di Dio e Ruggi D'Aragona", Salerno, Italy

⁴Department of Diagnostic Imaging, Scuola Medica Salernitana, University Hospital "San Giovanni di Dio e Ruggi D'Aragona", Salerno, Italy

Correspondence

Fabrizio Esposito, Department of Medicine, Surgery and Dentistry, Scuola Medica Salernitana, University of Salerno, Via S. Allende, Baronissi, 84081 Salerno, Italy.
Email: faesposito@unisa.it

Abstract

Age-related hearing loss (HL) can be related to brain dysfunction or structural damage and may result in cerebral metabolic/perfusion abnormalities. Arterial spin labeling (ASL) magnetic resonance imaging (MRI) allows investigating noninvasively brain perfusion changes. Pseudocontinuous ASL and T1-weighted MRI (at 3 T) and neuropsychological testing (Montreal Cognitive Assessment) were performed in 31 HL (age range = 47–77 years, mean age \pm SD = 63.4 \pm 8.4 years, pure-tone average [PTA] HL > 50 dB) and 28 normal hearing (NH; age range = 48–78 years, mean age \pm SD = 59.7 \pm 7.4 years) subjects. Cerebral blood flow (CBF) and gray matter volume (GMV) were analyzed in the cortical volume to assess perfusion and structural group differences. Two HL subjects showing cognitive impairment were excluded from group comparisons. No significant differences in either global or local atrophy were detected between groups but the HL group exhibited significant regional effects of reduced perfusion within the bilateral primary auditory cortex, with maximal CBF difference (–17.2%) in the right lateral Heschl's gyrus. For the whole sample of HL and NH subjects ($n = 59 = 31$ HL + 28 NH), the regional CBF was correlated positively to the regional GMV ($p = 0.020$). In HL subjects ($n = 31$), the regional CBF was correlated negatively to the audiogram steepness (frequency range: 2–4 kHz, right ear: $p = 0.022$, left ear: $p = 0.015$). The observed cortical pattern of perfusion reduction suggests that neuronal metabolism can be related to HL before the recognition of brain structural damage. This also illustrates the potential of ASL-MRI to contribute early functional markers of reduced central processing associated with HL.

KEYWORDS

arterial spin labeling, auditory cortex, brain atrophy, cerebral perfusion, hearing loss

1 | INTRODUCTION

Hearing loss (HL) is clinically characterized by audiometric threshold shifts, possibly causing deterioration in auditory processing, for example, speech perception and understanding, especially in noisy environment (Lee, 2013). Pathological changes associated with HL are mainly observed in the auditory periphery, as HL typically presents an irreversible loss of sensory hair cells and neurons in the cochlea (Huang & Tang, 2010; Kidd & Bao, 2012; Schuknecht & Gacek, 1993). However, concomitant functional and structural changes along the central auditory pathway and in the cerebral

cortex have been repeatedly reported in HL populations (see, e.g., Mazelová, Popelar, & Syka, 2003).

From the structural perspective, in a large longitudinal morphometric magnetic resonance imaging (MRI) study, Lin et al. (2014) reported an accelerated gray matter volume (GMV) reduction in HL subjects, compared to normal hearing (NH) controls, a phenomenon that occurred both globally (over the whole brain) and, locally, within the right temporal lobe, suggesting how auditory deafferentation eventually evolves toward a central (cortical) brain damage.

From the functional perspective, HL patients have been shown to exhibit decreased cognitive performances (Lin, Thorpe, Gordon-Salant, &

Ferrucci, 2011) and a higher risk for developing dementia and neurodegenerative disorders (Gates et al., 2010; Golub, 2017; Lin et al., 2011). Previous blood oxygen level dependent (BOLD) functional MRI (fMRI) studies have shown a reduced cortical activation in response to tonal stimulation in the tonotopic areas of the auditory cortex (Langers, van Dijk, Schoenmaker, & Backes, 2007; Zhang, Geng, Zhang, Li, & Zhang, 2006), especially at middle and higher frequencies (3.2 and 6.4 kHz) (Wolak et al., 2017), substantially mirroring the peripheral impairment of HL patients onto the auditory central perception. More recently, BOLD-fMRI studies conducted without stimulations (resting state; see, e.g., Chen et al., 2018) have similarly highlighted a significant reduction of spontaneous neural activity in the primary and secondary auditory cortex of HL patients which correlated with the reduced cognitive performances (including, e.g., language processing).

Finally, from the metabolic perspective, using ^{18}F -fluro-deoxy-glucose (FDG) positron Emission Tomography (PET), Verger et al. (2017) have revealed a specific pattern of decreased regional cerebral blood flow (CBF), a quantitative measure of baseline neuronal metabolism, in the associative auditory cortex of HL patients (mainly in the right hemisphere). While HL is frequently caused by accumulated noise and ototoxic experiences that produce a loss of sensory cells in the cochlea (Kurabi, Keithley, Housley, Ryan, & Wong, 2017), a possible reduction in the regional CBF in the auditory cortex may also indicate the presence of a vascular dysfunction, which could lead itself to neuronal deficits. In fact, because CBF is regulated according to local neuronal activity and metabolism (i.e., neurovascular coupling; Iadecola, 2017), if CBF deficiency is prior to neurodegeneration, a reduced CBF in the central auditory system of HL patients could be linked to a reduced dilatory capacity of cerebral vasculature in upregulating perfusion, with an increased risk for vascular disease and a higher vulnerability for neurological disorders in aging (Gao et al., 2013).

In the light of these evidences, it has become of outmost importance to search for functional alterations of the auditory "baseline" activation as possible early functional markers of central damage associated with HL, and to link these signs with structural and audiological measures as well as other clinical signs of neuronal degeneration.

Although PET imaging provides the clinical gold standard for the absolute quantification of regional brain metabolism at baseline, analogous regional CBF images can be nowadays acquired, even during routine MRI examinations, using arterial spin labeling (ASL) techniques (Alsop et al., 2015; Detre, Rao, Wang, Chen, & Wang, 2012; Telischak, Detre, & Zaharchuk, 2015). Differently from PET, which requires the injection of radioactive tracers, ASL-MRI uses arterial blood water as an endogenous tracer to provide regional CBF (perfusion) measurements over the whole brain on a voxel-by-voxel basis at the same spatial resolution of BOLD-fMRI, yielding an alternative fMRI marker of the baseline neuronal metabolism of brain tissues (Telischak et al., 2015). Moreover, compared to BOLD-fMRI contrast, regional CBF mapping with ASL-MRI has a higher spatial specificity for baseline neural activity and, similar to PET, allows an absolute quantification of this parameter (Chen, Jann, & Wang, 2015), which makes it well suited to detect early changes in neuronal function without any specific stimulation applied. For example, using ASL-MRI, Chao et al. (2010) have shown that brain hypoperfusion can predict clinical, functional, and cognitive decline, and

is therefore particularly useful for an early detection of the presence of a neurodegenerative disease. Moreover, even without any external specific acoustic stimulation (apart from the intrinsic acoustic stimulation provided by MRI scanner noise), and using the pseudocontinuous ASL (PCASL) variant, Gardumi, Ivanov, Havlicek, Formisano, and Uludağ (2017) have nicely delineated an extended high-perfusion signal in the human primary auditory cortex of NH subjects, suggesting that the primary sensory areas of the auditory cortex are likely characterized by a relatively high density of microvascularization, which could in principle make the PCASL technique particularly sensitive to detect early HL-related functional changes in the primary auditory cortex.

At present, due to its higher labeling efficiency, the PCASL is also the recommended ASL implementation for clinical studies (Alsop et al., 2015; Dolui et al., 2017) and can be suitably combined with a 3D readout acquisition scheme (3D-PCASL) to achieve optimal signal-to-noise ratio performances (Vidorreta et al., 2013).

The main purpose of this study was to investigate the possible relation between an early diagnosed HL condition (i.e., first symptoms reported in first audiological examination dated back to less than a few months) and baseline perfusion of the brain. Using a clinical implementation of the 3D-PCASL on a 3 T MRI scanner, the regional CBF was assessed in a group of HL patients and NH controls and the obtained perfusion measurements were related to structural MRI and audiological parameters.

2 | MATERIALS AND METHODS

2.1 | Subjects

Thirty-one HL patients (age mean = 63.4, $SD = 8.4$ years, range = 47–77; 20 males) were enrolled in the study without randomization. All patients involved were at the stage of their first clinical diagnosis of HL. All of them were complaining about hypoacusia since a few months or less. None of them used hearing aids before taking part in the study. HL was evaluated with pure-tone audiometry (Davies, 2016) and audiometric thresholds for air conduction were obtained at the frequencies of 0.25, 0.5, 1, 2, 4, and 8 kHz. The measurements were carried out in a soundproof chamber using a clinical audiometer. The audiogram curves with the full frequency characterization of each patient are shown in Figure 1a. PTA was calculated as recommended for the classification of HLs by The Bureau International d'Audiophonologie (BIAP, 2005) for 0.5, 1, 2, and 4 kHz (www.biap.org). The mean PTA of the enrolled HL patients was 55.5 ± 11.1 dB in the right ear and 53.4 ± 10.9 dB in the left ear. The "steepness" of the audiogram in (dB/octave) was computed for each pair of adjacent frequencies as the difference in hearing level (measured in dB) divided by the frequency difference (measured in octaves; König, Schaette, Kempter, & Gross, 2006):

$$S(i) = \frac{HT(f_{i+1}) - HT(f_i)}{\log_2 f_{i+1} - \log_2 f_i}$$

where $HT(f_i)$ is the HL threshold in dB at the frequency f_i and $f_i \in [0.25, 0.5, 1, 2, 4, 8]$ kHz and $S(i)$ is the steepness of the audiogram between frequency f_{i+1} and f_i .

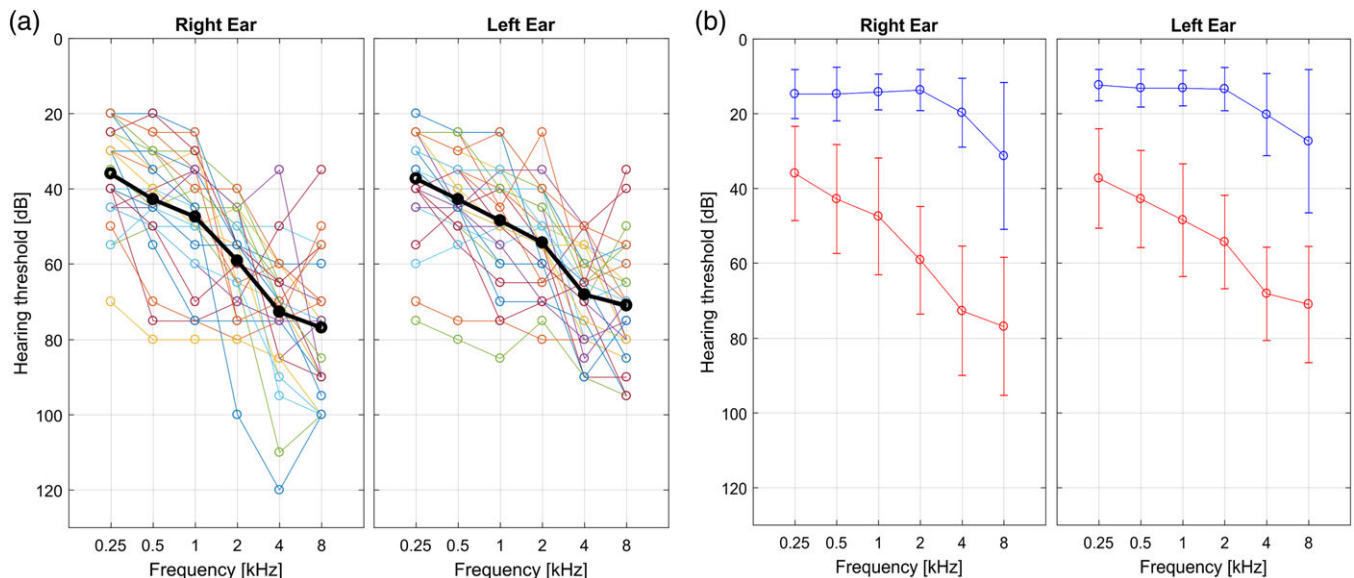


FIGURE 1 (a) Hearing loss (HL) characterization of each patient in right and left ear respectively. (b) Mean and SD across HL (red) and normal hearing (NH; blue) subjects of the hearing thresholds for both ears. The thresholds were assessed at six different frequencies with pure tone audiometry [Color figure can be viewed at wileyonlinelibrary.com]

Twenty-eight NH controls (age mean = 59.7, SD = 7.4 years, range = 48–78; nine males) and with no medical history of HL (or complain about their hearing) were included in the study. Figure 1b shows the mean audiogram curves (and SD bars) in the two groups in right and left ear, respectively. No randomization was used.

None of the subjects involved had any history of neurological and/or psychiatric disorders, surgical interventions in the ear, or MR contraindications. Subjects with a previous report of vascular dysfunction or with a history of stroke were not admitted to the study. As generalized microvascular alterations are to be anyway expected in these cohorts, a semiquantitative evaluation of white matter hyperintensities (a routinely used clinical marker of microvascular cerebral damage) was performed on the T2-weighted fluid attenuation inversion recovery (FLAIR) images (see Section 2.2) of all individuals by two experienced neuroradiologists blinded to the group membership. The amount of these lesions was quantified separately for the deep and periventricular white matter on the four-stage Fazekas scale (Fazekas, Chawluk, Alavi, Hurtig, & Zimmerman, 1987).

A list of daily taken medications (for chronic disorders) was recorded from each subject, and thereby four major categories were individuated: hypertension, prostate, cholesterol, and heart medications. As even a simple caffeine consumption can substantially decrease ASL-derived global perfusion levels, and such decreased levels can persist for about 75 min from intake before returning to baseline (see, e.g., Addicott et al., 2009; Clement et al., 2017), none of subjects was allowed to take caffeine (or any other medications) for at least 120 min before MRI scan. As all subjects were engaged in audiological and neuropsychological testing during the time between their arrival at the center and the start of the MRI scan, they could be closely and specifically monitored for this aspect. The possible effect of daily caffeine consumption was also controlled by asking for the estimated quantity of coffee as mean number of cups per day.

All participants were submitted to the Montreal Cognitive Assessment (MOCA; Nasreddine et al., 2005) for screening of cognitive

performances on the same day of (immediately before) the MRI examination.

The study was carried out in accordance with The Code of Ethics of the World Medical Association (Declaration of Helsinki) for experiments involving humans and the local ethical committee approved the study. A written informed consent was signed by each participant before MRI acquisition.

All the investigators knew the group allocation before (and during) the experiment and in performing the neuropsychological testing and the image data analyses (no blinding was done).

2.2 | MRI acquisition

Brain images were acquired using a 3 T MRI scanner (Siemens MAGNETOM Skyra; Siemens Healthcare, Erlangen, Germany), equipped with a head and neck (16 + 4 channel) radiofrequency coil supplied by the manufacturer. The imaging protocol included the following sequences:

- 3D T1-weighted magnetization prepared rapid gradient echo (MPRAGE) sequence with repetition time (TR) = 2,400 ms, echo time (TE) = 2.25 ms, resolution = $1 \times 1 \times 1 \text{ mm}^3$, matrix size = 256×256 , anterior–posterior phase-encoding direction, generalized autocalibrating partially parallel acquisitions (GRAPPAs) factor of 2 in phase-encoding direction. The MPRAGE scan was used for anatomical reference and morphometric analyses.
- A prototype 3D-PCASL sequence with TR = 4,600 ms, TE = 15.6 ms, field of view $192 \times 192 \text{ mm}^2$; slice thickness 3 mm, resolution = $3 \times 3 \times 3 \text{ mm}^3$, bolus duration 1,500 ms, postlabeling delay 1,500 ms, six repetitions, M0 prescan, 42 slices, turbo factor 14, echo-planar imaging (EPI) factor 21, number of segments 6 (total acquisition time = 6 min). The 3D-PCASL sequence employs the 3D GRASE readout module and implements a pseudocontinuous labeling scheme with background suppression as described in Dai, Garcia, De, and Alsop (2008); Dai, Robson,

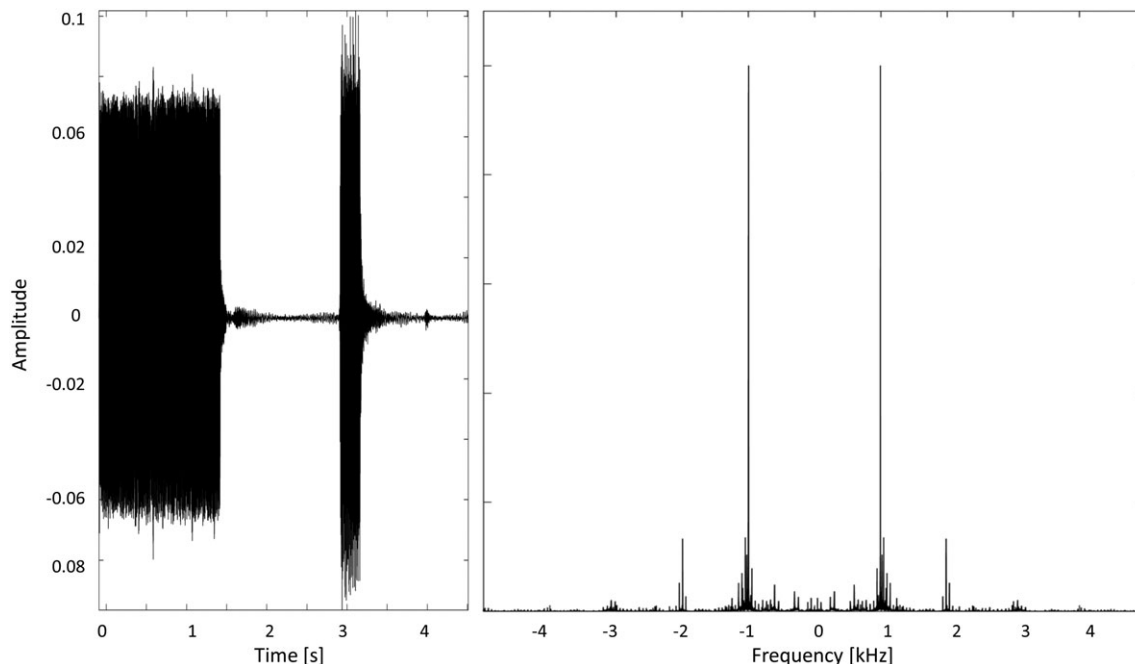


FIGURE 2 3D-pseudocontinuous arterial spin labeling (PCASL) acoustic stimulation in each repetition time (TR); signal in time domain (left); and in frequency domain (right)

Shankaranarayanan, and Alsop (2012); and Wu, Fernández-Seara, Detre, Wehrli, and Wang (2007). In each repetition of the sequence (TR), the tagging module and the EPI train causes an acoustic stimulation with a principal spectral contribution at 1 and 2 kHz (Figure 2). This series was acquired with the subject at rest with eye open.

- 3D T2-weighted FLAIR sequence with TR = 5,000 ms, TE = 387 ms, inversion time (TI) = 1800 ms, resolution = $0.6 \times 0.6 \times 1 \text{ mm}^3$, matrix size = 384×384 , sagittal orientation, anterior–posterior phase-encoding direction, GRAPPA factor of 2 in phase-encoding direction. The FLAIR scan was used for white matter hyperintensity analysis.

2.3 | Image analysis

Single-subject whole-brain CBF maps were calculated from the 3D-PCASL raw images using the prescan M0 image and the perfusion-weighted series using the calibration formula in Alsop et al. (2015) (provided by the inline scanner software).

For the group-level analysis, the single-subject CBF maps were spatially normalized using the SPM12 toolbox (www.fil.ion.ucl.ac.uk/spm/) running on MATLAB R2017a (The MathWorks, Inc., Natick, MA, www.mathworks.com) to the Montreal Neurological Institute (MNI) standard template (Evans et al., 1993) using a three-step procedure: First, the control images from the 3D-PCASL series were averaged to obtain an image with enhanced contrast, which was aligned in each subject to the corresponding anatomical 3D T1w image with an affine transformation. Second, all T1w images were segmented and normalized into a study specific template space with the nonlinear diffeomorphic DARTEL approach (Ashburner, 2007) and then transformed to the MNI space. Third, the initial affine transformation, the

DARTEL estimated nonlinear deformation fields and an isotropic 6-mm full width at half maximum (FWHM) Gaussian kernel were applied to the CBF maps of each subject. Besides CBF maps, GMV and white matter volume (WMV) maps were also obtained in the MNI space from the “unified” segmentation of T1w images (also requested by the DARTEL procedure; Ashburner & Friston, 2005) by spatially smoothing (with the same isotropic 6-mm FWHM Gaussian kernel) and modulating (to compensate the effect of warping on the intensity) the spatially normalized tissue probability images in such a way to preserve the total amount of signal from each region. From this segmentation, the total intracranial volume (ICV) was also estimated for each subject using the SPM12 utility function “tissue volumes.” In addition to the absolute CBF maps, because differences in regional CBF can also be attributable to differences in tissue composition (partial volume effect), a partial volume (PV) model was also considered to separate within-voxel gray matter (GM) and white matter (WM) CBF components and to account for the spatially variable mixing of GMV and WMV at each voxel. To this purpose, a validated spatial linear regression model of GM and WM CBF components with a fixed 3D kernel of $3 \times 3 \times 3$ voxels (Zhao et al., 2017) was applied (on the maps already in MNI space) as described in Asslani, Borogovac, and Brown (2008), thereby new regional CBF values could be calculated from the estimated GM CBF component. A more extended kernel of $7 \times 7 \times 7$ voxels was also considered to verify the impact of the kernel setting on the results. For the PV corrections, single subject GM masks were obtained by applying a fixed threshold to the tissue probability maps. For GM masking, only voxels with a GM probability higher than 0.2 were selected. An analysis of covariance was performed to assess the effect of age (as continuous covariate) and group (NH vs. HL) on the size of the GM masks.

In the MNI space, general linear models (for post hoc *t* tests) were computed voxel wise to compare GMV maps between the two

groups, while accounting for total ICV, sex, and age of each subject. The resulting statistical maps (t maps) were thresholded at $p = 0.05$ with a family wise error correction for multiple voxel-level comparisons using either the entire brain (whole brain correction) or the bilateral auditory cortex as search volume (small volume correction). For the “small volume” correction, an anatomical mask was defined on the MNI template according to a cytoarchitectonic atlas of the auditory cortex (Kim et al., 2000). Besides the anatomical masking of auditory cortical regions, this atlas provides a detailed cortical parcellation of the primary auditory areas as shown in Figure S1, Supporting Information (after projection on the cortical surface reconstruction of the right hemisphere of the MNI template, see next paragraph).

After spatial normalization, all individual CBF maps were imported in BrainVoyager (Brain Innovation, Maastricht, The Netherlands, www.brainvoyager.com) and further transformed to the Talairach space. This step allowed the analysis and presentation of group-level CBF data both in the volume and in the surface space on the cortical surface meshes reconstructed from the Talairach-transformed MNI template. The cortical parcellation of the primary auditory cortex was also overlaid to these meshes. In this common brain space, using BrainVoyager tools and plugins, group-level averaging, and general linear models (for post hoc t tests with correction for global CBF, age, and sex effects) were computed. The correction for global CBF was performed by first computing the mean absolute CBF over the entire brain mask in each subject and then adding the series of individual global CBF values as confound in the GLM. The t maps resulting from the post hoc t tests were then applied a minimum cluster size threshold estimated with Monte Carlo simulations (Forman et al., 1995; Goebel, Esposito, & Formisano, 2006). This approach allowed setting the extension of significant clusters using a nonparametric statistical approach, that is, independently of the spatial distribution of the estimated effects around each peak. In more detail, starting from either $p = 0.001$ or $p = 0.005$ as “cluster-forming” voxel-level thresholds, the threshold was first applied to all voxels; then, the minimum cluster size was set in such a way that an average of 5% false positive clusters falling within the search volume were counted in 1000 randomly generated images to which the same threshold was applied. To match the level of smoothness between the real map and the simulated maps, following the random number generation at each voxel, the resulting maps were spatially filtered with a Gaussian kernel at the FWHM initially estimated from the real map according to the 3D extension of the formula in Forman et al. (1995). The effect size, the level of variability in each group (SD), and the % statistical power were obtained, along with the peak of the effects, as post hoc estimates using the ClinCalc interactive web tool (<http://clincalc.com>).

Besides the above described atlas from Kim et al. (2000) (here used for cortical masking and for detailed cortical parcellation of the primary auditory areas), other two atlases were imported. One, from Mutsaerts et al. (2015) with the purpose to demarcate the three main perfusion territories supplied by the anterior, middle, and posterior cerebral arteries (MCA), each divided into a proximal, an intermediate and a distal vascular territory (according to previously estimated arterial transit times). The other, the automated anatomical labeling atlas (Tzourio-Mazoyer et al., 2002) was imported and used to locate additional cortical regions beside the auditory cortex. The voxel-wise

analysis (and the cluster-level correction for multiple comparisons) was replicated using a mask (the medial occipital cortex) of a cortical location potentially unaffected by HL, as searching region.

Region of interest (ROI) analyses were also performed: (a) to assess the coexisting effects of HL, age, and sex on the regional CBF; (b) to assess the hemispheric laterality of the regional CBF; (c) to correlate regional CBF with structural (regional GMV) and clinical (HT, S) measures; and (d) to analyze regional CBF outside of the auditory cortex. To jointly test for the presence of age and sex effects in combination with HL-related effects, the uncorrected regional CBF values were entered into a 3-ANOVA model with age, sex, and HL specified as separate as between-subject factors of interest. To assess the laterality, a two-way ANOVA (2-ANOVA) model with side (left, right) and HL condition, respectively, as within- and between-subject factors was applied to the mean regional CBF values in the anatomically defined regions taken separately from the right (mask size 38,466 mm³) and left (mask size 37,368 mm³) primary auditory cortex. To investigate the correlation between regional CBF and GMV in the whole group, and the correlation between the regional CBF and the audiogram thresholds and steepness (HT, S) in the HL group, a robust (weighted) multilinear regression model was applied, after accounting for sex and age. This analysis was performed in MATLAB R2017a (The MathWorks, Inc.) with the function *robustfit* and default settings (iteratively reweighted least squares with a bisquare weighting function).

Finally, to assess the local CBF alteration in a cortical area outside the auditory cortex, the mean CBF values were calculated in the medial occipital cortex (mask size 54,297 mm³) and compared (both the corrected and uncorrected data for global CBF) between the groups in a 3-ANOVA with age, sex, and group as factors.

3 | RESULTS

3.1 | Clinical data

According to the available audiograms, the highest steepness value was observed in the frequency range between 2 and 4 kHz in the (relative) majority of HL patients (43.3% in the right ear, 36.7% in left ear).

According to the neuropsychological testing, 29/31 HL patients were cognitively intact (MOCA total score > 15.5, after correction for age and education). Two HL patients (and none of the NH controls) obtained a MOCA total score below the clinical cut-off of 15.5 and were therefore excluded from the voxel-wise group comparisons in the neuroimaging data analysis.

There were no significant differences between groups in the daily amount of caffeine consumption. The use of hypertension, prostate, and heart medication was not more frequent in any of the two groups compared to the other. Cholesterol medications were more frequent in the HL group ($n = 12$) compared to the NH group ($n = 1$; chi-squared test: $p = 0.007$).

In the semiquantitative MRI evaluation of white matter lesions, compared to the NH group, the HL group exhibited increased Fazekas

TABLE 1 CBF mean values \pm SD from the uncorrected CBF maps and the PV corrected (kernel 3 and 7 voxels), respectively, calculated in the peak of the hypoperfused region in the right PAC, over the entire cluster in the right PAC, and over the whole GM (using individual masks). In the last column, the statistical significance (p -value) of the difference between the two groups (HL vs. NH) is also reported

	Data	NH	HL	Difference (p -value)
Local peak in right PAC	CBF (mL/100 g/min)	47.9 \pm 9.7	39.7 \pm 9.3	$p = 0.0017$
	GM CBF (mL/100 g/min; PV kernel 3 voxels)	131.4 \pm 29.0	112.4 \pm 27.3	$p = 0.013$
	GM CBF (mL/100 g/min; PV kernel 7 voxels)	95.3 \pm 16.2	82.6 \pm 15.8	$p = 0.004$
Cluster in the right PAC	CBF (mL/100 g/min)	47.8 \pm 9.6	39.6 \pm 9.3	$p = 0.0019$
	GM CBF (mL/100 g/min; PV kernel 3 voxels)	123.0 \pm 26.6	106.3 \pm 24.3	$p = 0.017$
	GM CBF (mL/100 g/min; PV kernel 7 voxels)	97.3 \pm 17.4	85.2 \pm 16.9	$p = 0.01$
Whole GM (individual masks)	CBF (mL/100 g/min)	36.6 \pm 8.1	33.3 \pm 8.2	$p = 0.13$
	GM CBF (mL/100 g/min; PV kernel 3 voxels)	87.7 \pm 18.5	79.4 \pm 20.3	$p = 0.11$
	GM CBF (mL/100 g/min; PV kernel 7 voxels)	79.3 \pm 17.5	71.7 \pm 18.9	$p = 0.12$

CBF = cerebral blood flow; GM = gray matter; HL = hearing loss; NH = normal hearing; PAC = primary auditory cortex.

scores in the deep white matter (Wilcoxon rank sum test: $p = 0.025$) but not in the periventricular white matter.

3.2 | Neuroimaging data

There were no significant differences between HL and NH groups in the global perfusion level (mean CBF over the whole brain) and global atrophy (mean GMV over the whole brain). Similarly, when extending the voxel-wise statistical comparisons to all brain voxels (i.e., with no anatomical mask applied); there were also no significant differences between HL and NH groups.

To specifically test for any regional effects within the entire bilateral auditory cortex, a bilateral anatomical mask was applied to restrict to search volume of voxel-wise comparisons to all primary auditory regions from both hemispheres according to the atlas parcellation (see Figure S1, Supporting Information). Even in this case, no clusters were found with significant regional GMV differences. In contrast, one cluster (size 327 mm³) of significant regional CBF differences emerged in the right primary auditory cortex in which HL patients exhibited a significantly reduced regional CBF in comparison to NH subjects (peak effect size: -8.2 [mL/100 g/min] corresponding to -17.2% , cluster-forming threshold $p = 0.001$). These regional CBF differences remained statistically significant after applying individual GM masks to the ASL images and correcting the individual CBF maps at each voxel for partial volume effects prior to recalculating the GM-specific CBF estimates for each group. There was a significant effect of age ($p = 0.0009$) in the size of whole GM masks but this size was not significantly different between NH and HL groups after correcting for age, nor the number of GM voxels was different across subjects in the detected cluster of reduced CBF (all voxels in this cluster had a GM probability higher than 0.2 in all subjects). After PV correction, only the GM-specific CBF estimates in this cluster, not the whole GM-specific CBF estimates, were significantly different between NH and HL groups (Table 1).

Moreover, a 3-ANOVA analysis of the age- and sex-uncorrected regional CBF values confirmed a significant main effect of both HL ($p = 0.0001$) and age ($p = 0.0048$), as expected for age-related HL, but not a significant effect of sex ($p = 0.2074$), ruling out that the reported HL effects could be biased by the different proportions of males and females in the two groups.

The local peak of this hypoperfusion effect, corresponding to the highest regional perfusion reduction (see also Table 1) was located inside the lateral Heschl's gyrus of the right hemisphere (Figure 3). However, starting from a slightly less conservative cluster-forming voxel-level threshold ($p = 0.005$), the same regional effects of reduced regional CBF in HL patients emerged as two bilateral clusters in the Heschl's gyri and one additional cluster in the left superior temporal gyrus, encompassing both the proximal and the MCA perfusion territories (Figure 4). Contrariwise, no regional GMV differences emerged from the comparison between NH and HL groups over the same anatomical mask, using the same uncorrected voxel-level thresholds ($p = 0.001$ or $p = 0.005$) and the same minimum cluster size thresholds applied for the detection of regional CBF differences.

Figure 5 displays the voxel-wise averaged whole-brain CBF maps, calculated separately for the NH ($n = 28$) and HL ($n = 29$) groups after spatial normalization to the common brain (MNI template) and after correcting the absolute values for the global CBF. In addition, two representative single-subject CBF maps (one per group) are shown in Figure S2, Supporting Information. To improve the comparative display, an identical range and pseudocolor scaling was applied to the perfusion values and the group maps were overlaid both on a triplanar volumetric view (centered at the exact peak of regional hypoperfusion) and on the reconstructed cortical surface mesh of the right hemisphere of the MNI template anatomy. In this way, the maps were further reminiscent of a spatially distributed cortical pattern of reduced perfusion levels in the HL group, with regional effects being maximal inside, but also extending far beyond, the primary auditory cortex. Namely, the trend of reduced averaged perfusion seems to involve both secondary auditory regions (within the temporal lobe) and multiple extra-auditory regions in the parietal and prefrontal cortex. Moreover, relatively higher average CBF levels are observed in the right primary auditory cortex in both NH and HL groups in comparison to the left primary auditory cortex. Thereby, to further explore the possible "intrinsic" laterality of the regional CBF, the entire left and right auditory cortex from the same anatomical mask were also considered separately and the regional CBF values from all subjects in each group were averaged over the entire right and left auditory cortex. In this case, a statistically significant laterality effect was detected, with higher regional CBF values in the right versus left hemisphere in

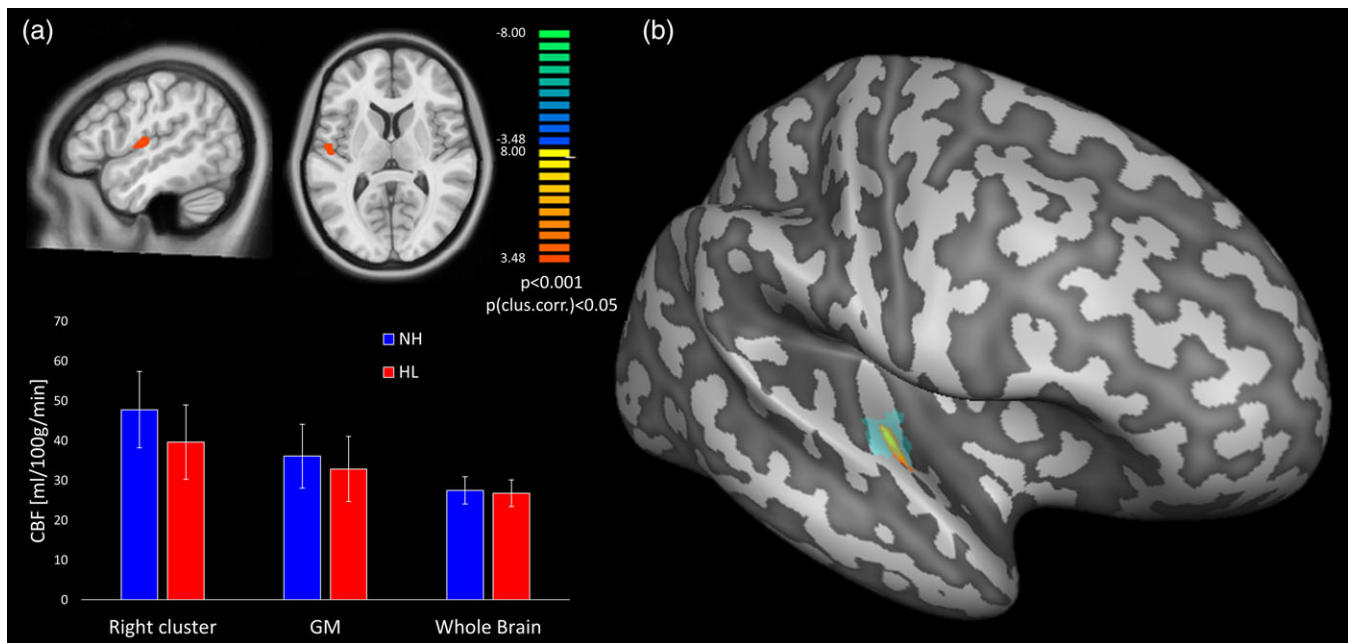


FIGURE 3 (a) Statistical t maps of the voxel-based comparison between hearing loss (HL) and normal hearing (NH; $p < 0.05$, cluster-level corrected for multiple comparison in the bilateral primary auditory cortex as search volume) and bar plots of the mean cerebral blood flow (CBF; PV uncorrected) with SD bars for the two groups in: (i) the significant cluster in the right primary auditory cortex, (ii) the whole GM, and (iii) the whole brain (i.e. WM + GM + CSF). (b) Projection of the significant cluster, and of the anatomical location of the lateral Heschl's gyrus, on the reconstructed surface mesh of right hemisphere of the MNI template [Color figure can be viewed at wileyonlinelibrary.com]

both HL and NH groups ($p < 0.001$) and no group by side interaction ($p > 0.05$). To confirm that the local CBF alteration is only confined in the auditory cortex, the whole-brain and ROI analysis were replicated in the media occipital cortex. In this case, no significant

differences were found between the two groups (mean absolute CBF right: HL = 34.12 mL/100/min, NH = 37.21 mL/100 g/min; mean absolute CBF left: HL = 33.21 mL/100/min, NH = 37.00 mL/100 g/min, $p > 0.05$).

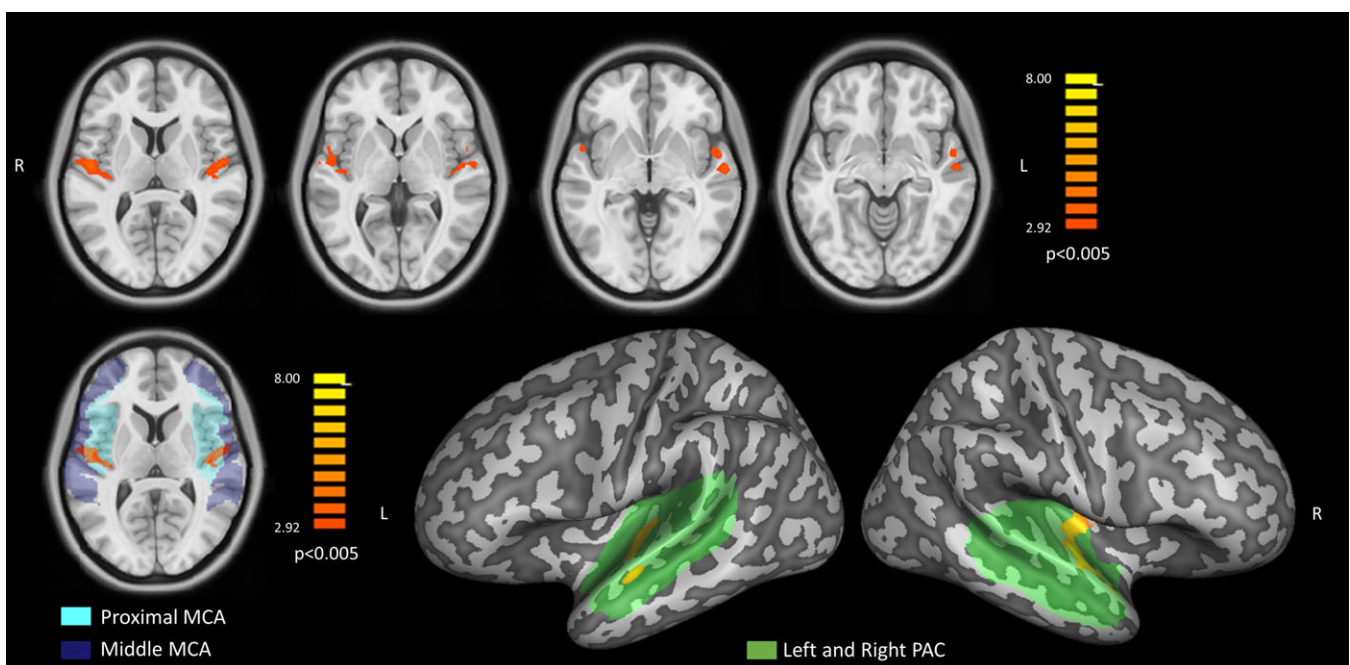


FIGURE 4 Upper row: statistical t maps of the bilateral effects in the voxel-based comparison between hearing loss (HL) and normal hearing (NH; $p < 0.005$). Bottom left: single slice view of the same statistical t map showing the bilateral effect with the proximal (cyan) and middle (blue) perfusion territories supplied by the middle cerebral arteries (MCAs) superimposed in transparency. Bottom right: projection of the same statistical t map, on the MNI surface meshes with the anatomical mask of the primary auditory cortex (PAC) superimposed in green transparency [Color figure can be viewed at wileyonlinelibrary.com]

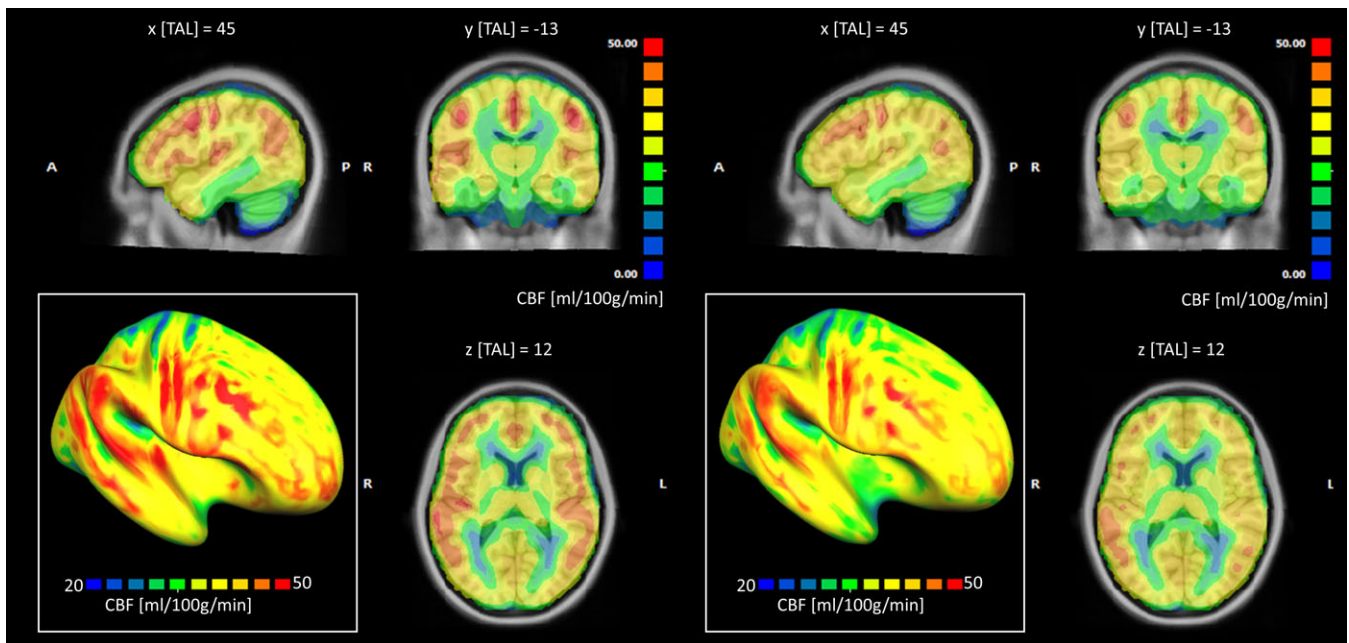


FIGURE 5 Group-averaged whole-brain cerebral blood flow (CBF) maps calculated after correcting the absolute values for the global CBF, for the normal hearing (NH) group (left panel) and the hearing loss (HL) group (right panel) displayed on a triplanar volumetric view after scaling between 0 and 50 mL/100 g/min. In the left-bottom inset of each panel, the same maps have been projected onto the surface mesh of the right hemisphere and rescaled between 20 and 50 mL/100 g/min [Color figure can be viewed at wileyonlinelibrary.com]

Finally, when extracting mean regional values from each individual in the above cluster in the right primary auditory cortex, the robust linear regression analysis highlighted a positive correlation between regional CBF and GMV (after correction for sex, age, and global values of both measures). This effect was maximally significant in the whole group of subjects ($n = 59$, $p = 0.02$), weakly significant in the HL group ($n = 31$, $p = 0.05$) and not at all significant in the NH group ($n = 28$, $p = 0.37$). Moreover, when considering the same regional values for all HL patients in combination with their own audiogram features, the regional CBF, but not the regional GMV, was negatively correlated with the HL steepness for both the right ($n = 31$, $r = -0.63$, $p = 0.022$, $r^2 = 0.21$) and of the left ($n = 31$, $r = -0.71$, $p = 0.015$, $r^2 = 0.24$) ears in the 2–4 kHz interval (Figure 6), whereas no significant correlations were found with the absolute HT for any frequencies and for both ears.

4 | DISCUSSION

The aim of the present study was to identify and characterize the possible association between HL and regional cerebral perfusion (CBF) using a clinical prototype 3D implementation of the PCASL sequence, and to possibly link such effects to structural MRI measurements (regional GMV) and audiogram features (audiogram HL thresholds and steepness).

In other clinical applications (e.g., Alzheimer disease [AD]), areas of reduced cerebral perfusion have been detected with ASL-MRI which were largely overlapping with regions of significant hypometabolism in ^{18}F -FDG PET study (Chen et al., 2011; Verfaillie et al., 2015), thereby suggesting that ASL-MRI might provide a useful noninvasive alternative to PET imaging, to quantify regional brain metabolism in

neurodegenerative diseases. In this study, the comparison between HL and NH groups, when conducted over all voxels of the auditory cortex, disclosed a significantly decreased CBF in the right primary auditory cortex, with a peak of perfusion reduction of 17.2% falling in the right lateral Heschl's gyrus, even when no significant differences were observed in the regional GMV from the same regions. Moreover, no significant local CBF depression was found when the analysis was

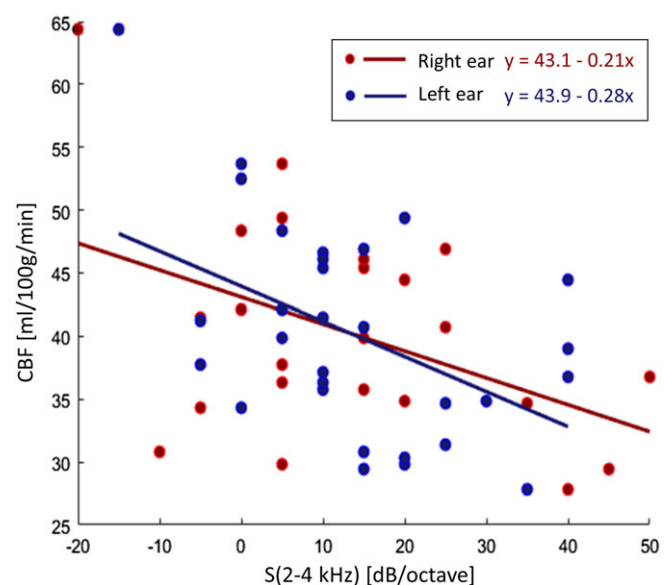


FIGURE 6 Scatter plot and linear trends (and line equations) of the correlations between the audiogram steepness (2–4 kHz) and the cerebral blood flow mean value in the cluster of significant difference between normal hearing and hearing loss (HL) [Color figure can be viewed at wileyonlinelibrary.com]

conducted on the voxels outside the primary auditory cortex (e.g., in the visual cortex), suggesting the presence of a spatially confined phenomenon.

The statistical significance of these differences was not substantially affected by the correction of partial volume effects from each individual CBF maps as calculated from the original 3D-PCASL series (with a fixed kernel of $3 \times 3 \times 3$ or $7 \times 7 \times 7$ voxels), nor it was biased by the different proportion of males and females in the two groups (males typically have higher HL rate than female). This distinctly suggests that the 3D-PCASL sequence has the potential to display decreased levels of functional activation or neuronal metabolism associated with the HL condition, even when structural MRI is not providing sufficient evidence for brain atrophy and beyond the impact of partial volume and gender effects on the original ASL signal. However, larger sample sizes and long-term follow-up (e.g., 6, 12, or 24 months) studies are, respectively, needed to validate the observed hypoperfusion effects outside the primary auditory cortex and to possibly address the prognostic value of this information with respect to naturally occurring or treatment-related modifications of the HL condition.

In agreement with the presented results, a recent PET study (Verger et al., 2017) conducted on late-onset deaf patients reported that the right auditory cortex was hypoperfused in HL patients, the obvious (matching) interpretation of these findings being that a functional narrowing of auditory cortical activity is occurring in association with the peripheral auditory dysfunction (Irvine & Rajan, 1996; Rajan, Irvine, Wise, & Heil, 1993). However, differently from the PET study, where the brain metabolism was also shown to increase in other regions outside the auditory cortex (especially at the vertex of the brain), our whole-brain CBF analysis did not provide evidence of CBF increase in HL patients and all statistically significant CBF alterations were strictly confined as regional effects within the primary auditory cortex (and additional trends toward possible hypoperfusion in parietal and prefrontal regions were also visible on the cortical pattern of average perfusion levels). One possible explanation of the divergent findings is that the patients involved in the PET study were all deaf for 7 years or longer whereas all patients involved in the present study were scanned upon their very first clinical assessment for possible HL. Thus, it seems plausible that, given the early status of hearing impairment of our patients, the neuroplastic reorganization of the whole brain metabolism hypothesized previously would not be manifest yet in our sample. In addition, our MRI study involved healthy subjects that have been enrolled as control group in the same study period of HL subjects, thus minimizing the role of concomitant factors that might have affected group comparisons. This might explain the lack of hyperperfused cortical regions at the brain vertex that have been found in the PET study.

On the other hand, although the selective reduction of ASL-derived perfusion levels in the primary auditory cortex persists after the correction for global CBF changes, it is not possible to exclude that some HL individuals might have confounding factors, related to a chronic pharmacological treatment or to the general vascular conditions, contributing to a more global reduction of ASL-derived perfusion levels. Indeed, we found that 12 HL subjects (vs. only one NH subject) made regular use of cholesterol medications, whereas all other types of chronic medications were balanced between groups. In

addition, the size and confluence of deep, albeit not periventricular, white matter lesions were larger in HL, compared to NH, subjects. In both cases, however, it is unlikely that these factors might have biased the search for selective reduction of ASL-derived perfusion toward the primary auditory cortex. In fact, the only current evidence for ASL-derived perfusion changes in relation to the chronic use of cholesterol medication points, not to decreases, but rather to increases in regional CBF (not in the auditory cortex) in persons at risk for AD (Carlsson et al., 2012). Moreover, recent work reported that periventricular, but not deep, white matter lesions were associated with regional cortical CBF reductions in elderly subjects at risk for cerebrovascular diseases (Bahrani et al., 2017).

It should be pointed out that the ASL settings used for the present study were not optimized to provide the highest sensitivity to regional CBF changes in relation to specific perfusion territories encompassing auditory or extra-auditory regions. Indeed, the highest effects of reduced CBF were found to putatively encompass two adjacent perfusion territories (middle and proximal MCA) whereas other potentially affected (extra-auditory) regions encompass different territories (i.e., with possibly different arterial transit times). Therefore, a different postlabeling delay would have potentially increased the sensitivity of the analysis. Although we used both a labeling duration (1,500 ms) and a postlabeling delay (1,500 ms) shorter than the values recommended in general for clinical (2D or 3D) PCASL studies (both 1800 ms) (Alsop et al., 2015), our labeling parameters were set identically to a previous 3D-PCASL study reporting hypoperfusion areas in AD patients and specifically suggesting that a postlabeling delay of 1,500 ms can be sufficient to display CBF with this ASL variant (Liu et al., 2015). Anyway, future and more advanced implementations of the same 3D-PCASL sequence, for example, allowing for multiple CBF images at different postlabeling times and the contextual estimation of the actual arterial transit times, will possibly contribute to increase the sensitivity of whole brain CBF analyses (Johnston, Lu, Maldjian, & Jung, 2015; Kramme et al., 2015).

The most significant reduction of the regional brain perfusion was confined to the right hemisphere, albeit additional effects were immediately visible within both the left and the right primary auditory cortex when slightly reducing the cluster-forming statistical threshold in the voxel-level analysis. Lateralized hypoperfusion is in line with the previous PET study (Verger et al., 2017) but also with structural morphometric findings of a lateralized atrophy in the right temporal lobe as emerging from a structural MRI follow-up of a large HL cohort (Lin et al., 2014). It should be also said, however, that, in line with our structural MRI results, at least three previous structural MRI cross-sectional studies did not report any evidence of atrophy in the temporal lobe of different HL cohorts (Alfandari et al., 2018; Boyen, Langers, de Kleine, & van Dijk, 2013; Husain et al., 2011).

A strictly related aspect, which could also at least partly explain this finding, is that the regional perfusion of the primary auditory cortex was intrinsically (and significantly) lateralized to the right hemisphere, independently of the hearing condition. A likely explanation for this lateralization is that the acoustic stimulation produced by the MRI scanner noise during the 3D-PCASL sequence, which consisted of identically repeated bursts of tonal sounds at the main frequency of 1 kHz, might have induced different baseline perfusion levels

between the right and the left auditory cortex. Indeed, previous BOLD-fMRI activation studies have exhaustively demonstrated that the left auditory cortex is generally more specialized for the “temporal” processing required for the perception of complex acoustic sounds (i.e., sounds that dynamically change their spectral features, such as, e.g., voices), whereas the right primary auditory cortex is more specialized for the “spectral” processing required for the perception of tonal stimuli (including music; Schonwiesner, Rübsem, & Von Cramon, 2005; Sininger & De Bode, 2008; Zatorre, Belin, & Penhune, 2002). Based on this notion, the intrinsic lateralization of the regional perfusion in the primary auditory cortex (in both HL patients and NH subjects) to the right hemisphere, and, consequentially, the greater size of the regional CBF alterations in HL patients (vs. NH subjects) observed in the right hemisphere, could be linked to the higher sustained functional activation elicited by the scanner acoustic noise produced by the MRI gradient system during the ASL scans. On the other hand, this explanation alone would not justify the above-mentioned homologous PET and structural MRI changes. More convincingly, it might be that the peripheral high-frequency-specific HL typically observed in aging-related HL can be related primarily to the cortical region specialized for the “spectral” processing with relative sparing of the left auditory cortex.

The intrinsically activated status of the auditory cortex during the MRI scan can also explain the generally higher sensitivity of ASL techniques in these regions, compared to other brain regions. In this sense, the HL condition studied here could in principle provide a (sort of) pathological model to investigate the functional activation elicited by the MRI scanner noise in relation to the ASL sequence settings (see Seifritz et al., 2006). However, as no significant correlations were found between the regional CBF and the audiometric pure-tone thresholds, not even at the most stimulated frequencies (1 and 2 kHz, see Figure 2), it is also likely that the acoustic stimulation produced by the MRI scanner only contributes to the right laterality of CBF patterns (and therefore to the lateralized sensitivity of CBF analysis) according to the above described mechanisms, but not (or at least not exclusively) to the observed reduction of the regional perfusion in the primary auditory cortex of HL patients.

To further investigate the nature of the reduced regional CBF in the primary auditory cortex, and to possibly highlight the structural and clinical correlates of this effect, the regional CBF values from all patients were correlated with the corresponding regional GMV measures and with the HL steepness of the audiometric curves.

Although no significant GMV differences were detected between HL and NH groups, which rules out that early diagnosed HL patients were significantly more atrophic than age-matched NH subjects, and having excluded that the observed differences were substantially driven by (structural-only) partial volume effects, here we found a statistically significant positive correlation between the regional CBF and GMV values for the detected cluster of hypoperfusion in the right primary auditory cortex. This might suggest that the observed reduction of the regional CBF could still be an early sign of neuronal loss in the cerebral cortex (Madhyastha et al., 2015), rather (or more) than simply being a reduced activation response to the acoustic stimulation produced by scanner noise, which would simply mirror an (irreversible) peripheral auditory dysfunction. Moreover, when considering the

steepness of the audiograms, a significant negative correlation was found between the regional CBF values and the audiogram steepness between 2 and 4 kHz, a range of frequency that does not encompass the main harmonic of the sound produced by the MRI scanner during the 3D-PCASL scan (centered at 1 kHz).

The steeply sloping high frequency loss is a highly typical audiological pattern of the age-related HL condition, which is sometimes also called “sloping” sensori-neural HL (see, e.g., Wolak et al., 2017). This pattern most frequently characterizes the HL impairment in the frequency interval between 2 and 4 kHz (Huang & Tang, 2010), often with a notch or dip around the 4 kHz region (Schuknecht & Gacek, 1993). A steep slope between two adjacent frequencies is therefore spotted as an audiological marker of discontinuity in the audiogram shape that can reflect corresponding discontinuities in the inner hair cells (Schecklmann et al., 2012), thereby it may represent a more specific sign of the initial (frequency selective) hearing damage. Indeed, this pattern was also characteristic of the HL patients studied here, for which the steepest slope occurred for the 2–4 kHz in the relative majority of the subjects for both ears, albeit the absolute pure tone thresholds were highly variable across subjects and between ears (and not significantly correlated with CBF). Thus, the observed patterns seem to reflect finer aspects (and provide more advanced clinical features) of the pathological HL condition, rather (or more) than displaying the simple reduction of the peripheral input at specific frequencies, thereby promoting the proposed MRI-based technique as a promising tool to detect more fine-grained signs of the central effects of HL.

In general, when functional deficits are associated with reduced local perfusion/metabolism in a brain region that is tightly linked to the affected (cognitive or sensorimotor) domain, it is not possible to mechanistically determine whether the cortical (CBF or GMV) change causes the impaired performance (as an effect of a neurovascular damage) or it is the low functional regime of the brain metabolism that triggers neuroplastic changes within the local tissue. Although we excluded from the HL group, not only subjects presenting overt dementia but also those with significant subclinical cognitive impairment (MOCA score < 15), to avoid the confounding effect of a primary diffuse (neurovascular/degenerative) cortical involvement, the possibility of a selection bias toward patients with a selective primary (neurovascular/degenerative) auditory cortex involvement cannot be ruled out completely. Therefore, the observed local perfusion/metabolism in the primary auditory cortex of the studied HL subjects could be in principle either triggered by the sensory deprivation implied by HL or vice versa. However, the most recent large-scale MRI study on cognitive aging and general cerebrovascular health conditions, using both structural and perfusion MRI with 3D PCASL, and properly accounting for age, sex, education, and occupation, as well as controlling for PET-derived global amyloid and composite tau burden as AD markers, clearly showed how systemic vascular health was associated with widespread cerebral hypoperfusion throughout the brain, whereas the regional perfusion in the primary auditory cortex (Heschl's gyrus) was not more associated with poorer cerebrovascular and metabolic conditions than other cortical regions within the frontal, cingulate, and parietal cortex (Vemuri et al., 2018). Considering also that age-related HL is strikingly common (affecting up to 70% of

normal population aged more than 70 years), the possibility of having selected a specific sample of patients with a selective primary vascular/neurodegenerative auditory cortex involvement appears unlikely. For this reason, even though a more reliable demonstration can be likely obtained only with a follow-up evaluation of samples with treated and nontreated HL, our current opinion is that the observed auditory cortical hypoperfusion reflects the peripheral dysfunction.

In conclusion, this study has presented the first application of an ASL-MRI technique to the brain perfusion analysis of the HL condition. The reported cortical pattern of reduced perfusion and the observed regional effects of central hypoperfusion within the primary auditory cortex associated with an early HL condition suggests that there is a link between cortical activation and neuronal metabolism and HL even if no structural damage (atrophy) is evident. Although further technical improvements are possible, and longitudinal studies on possibly larger samples of patients are required to validate this tool for the clinical application, the reported results from the currently available implementation of the 3D-PCASL may potentially contribute novel and early functional markers of reduced central processing associated with HL. Future studies are needed to combine this information with BOLD-fMRI activation experiments and a longitudinal investigation of the reported effects will be essential to monitor the HL condition over time in parallel with the neuropsychological outcome.

ACKNOWLEDGMENTS

The authors would like to thank Amplifon SpA. for supporting this research. The authors would also like to thank Nashiely S. Pineda-Alonso and Domenico Zacà from Siemens Healthcare for facilitating and supporting the use of the 3D-PCASL prototype sequence, and Federico De Martino and Faruk Gulban from Maastricht University for providing the anatomical parcellation of the primary auditory cortex.

CONFLICT OF INTERESTS

The authors declared no potential conflicts of interest with respect to the research, authorship, and/or publication of this article.

ORCID

Fabrizio Esposito  <https://orcid.org/0000-0002-5099-9786>

REFERENCES

- Addicott, M. A., Yang, L. L., Peiffer, A. M., Burnett, L. R., Burdette, J. H., Chen, M. Y., ... Laurienti, P. J. (2009). The effect of daily caffeine use on cerebral blood flow: How much caffeine can we tolerate? *Human Brain Mapping, 30*, 3102–3114.
- Alfandari, D., Vriend, C., Heslenfeld, D. J., Versfeld, N. J., Kramer, S. E., & Zekveld, A. A. (2018). Brain volume differences associated with hearing impairment in adults. *Trends in Hearing, 22*, 233121651876368. <http://journals.sagepub.com/doi/10.1177/2331216518763689>
- Alsop, D. C., Detre, J. A., Golay, X., Günther, M., Hendrikse, J., Hernandez-Garcia, L., ... Zaharchuk, G. (2015). Recommended implementation of arterial spin-labeled perfusion MRI for clinical applications: A consensus of the ISMRM perfusion study group and the European consortium for ASL in dementia. *Magnetic Resonance in Medicine, 73*, 102–116. <http://doi.wiley.com/10.1002/mrm.25197>
- Ashburner, J. (2007). A fast diffeomorphic image registration algorithm. *NeuroImage, 38*, 95–113. <http://linkinghub.elsevier.com/retrieve/pii/S1053811907005848>
- Ashburner, J., & Friston, K. J. (2005). Unified segmentation. *NeuroImage, 26*, 839–851. <http://linkinghub.elsevier.com/retrieve/pii/S1053811905001102>
- Asllani, I., Borogovac, A., & Brown, T. R. (2008). Regression algorithm correcting for partial volume effects in arterial spin labeling MRI. *Magnetic Resonance in Medicine, 60*, 1362–1371.
- Bahrani, A. A., Powell, D. K., Yu, G., Johnson, E. S., Jicha, G. A., & Smith, C. D. (2017). White matter hyperintensity associations with cerebral blood flow in elderly subjects stratified by cerebrovascular risk. *Journal of Stroke and Cerebrovascular Diseases, 26*, 779–786. <https://doi.org/10.1016/j.jstrokecerebrovasdis.2016.10.017>
- BIAP Recommendation 02/1: Audiometric Classification of Hearing Impairments. Liège (2005). <http://www.biap.org/en/recommandations/recommendations/tc-02-classification>
- Boyen, K., Langers, D. R. M., de Kleine, E., & van Dijk, P. (2013). Gray matter in the brain: Differences associated with tinnitus and hearing loss. *Hearing Research, 295*, 67–78. <https://doi.org/10.1016/j.heares.2012.02.010>
- Carlsson, C. M., Xu, G., Wen, Z., Barnet, J. H., Blazel, H. M., Chappell, R. J., ... Johnson, S. C. (2012). Effects of atorvastatin on cerebral blood flow in middle-aged adults at risk for Alzheimer's disease: A pilot study. *Current Alzheimer Research, 9*, 990–997. <http://www.eurekaselect.com/openurl/content.php?genre=article&issn=1567-2050&volume=9&issue=8&spage=990>
- Chao, L. L., Buckley, S. T., Kornak, J., Schuff, N., Madison, C., Yaffe, K., ... Weiner, M. W. (2010). ASL perfusion MRI predicts cognitive decline and conversion from MCI to dementia. *Alzheimer Disease and Associated Disorders, 24*, 19–27. <https://insights.ovid.com/crossref?an=00002093-201001000-00003>
- Chen, J. J., Jann, K., & Wang, D. J. J. (2015). Characterizing resting-state brain function using arterial spin labeling. *Brain Connectivity, 5*, 527–542. <http://online.liebertpub.com/doi/10.1089/brain.2015.0344>
- Chen, Y., Wolk, D. A., Reddin, J. S., Korczykowski, M., Martinez, P. M., Musiek, E. S., ... Detre, J. A. (2011). Voxel-level comparison of arterial spin-labeled perfusion MRI and FDG-PET in Alzheimer disease. *Neurology, 77*, 1977–1985.
- Chen, Y.-C., Chen, H., Jiang, L., Bo, F., Xu, J.-J., Mao, C.-N., ... Gu, J.-P. (2018). Presbycusis disrupts spontaneous activity revealed by resting-state functional MRI. *Frontiers in Behavioral Neuroscience, 12*, 1–12. <http://journal.frontiersin.org/article/10.3389/fnbeh.2018.00044/full>
- Clement, P., Mutsaerts, H. J., Václavů, L., Ghariq, E., Pizzini, F. B., Smits, M., ... Achten, E. (2017). Variability of physiological brain perfusion in healthy subjects – A systematic review of modifiers. Considerations for multicenter ASL studies. *Journal of Cerebral Blood Flow and Metabolism, 38*, 1418–1437.
- Dai, W., Garcia, D., De, B. C., & Alsop, D. C. (2008). Continuous flow-driven inversion for arterial spin labeling using pulsed radio frequency and gradient fields. *Magnetic Resonance in Medicine, 60*, 1488–1497.
- Dai, W., Robson, P. M., Shankaranarayanan, A., & Alsop, D. C. (2012). Reduced resolution transit delay prescan for quantitative continuous arterial spin labeling perfusion imaging. *Magnetic Resonance in Medicine, 67*, 1252–1265.
- Davies, R. A. (2016). Audiometry and other hearing tests. *Handbook of Clinical Neurology, 137*, 157–176. <https://www.sciencedirect.com/science/article/pii/B978044463437500011X>
- Detre, J. A., Rao, H., Wang, D. J. J., Chen, Y. F., & Wang, Z. (2012). Applications of arterial spin labeled MRI in the brain. *Journal of Magnetic Resonance Imaging, 35*, 1026–1037. <http://doi.wiley.com/10.1002/jmri.23581>
- Dolui, S., Vidorreta, M., Wang, Z., Nasrallah, I. M., Alavi, A., Wolk, D. A., & Detre, J. A. (2017). Comparison of PASL, PCASL, and background-suppressed 3D PCASL in mild cognitive impairment. *Human Brain Mapping, 38*, 5260–5273.
- Evans A.C., Collins D.L., Mills S.R., Brown E.D., Kelly R.L., Peters T.M. (1993). *3D statistical neuroanatomical models from 305 MRI volumes*. In 1993 I.E. Conference Record Nuclear Science Symposium and Medical Imaging Conference (pp. 1813–1817). <http://ieeexplore.ieee.org/lpdocs/epic03/wrapper.htm?arnumber=373602>
- Fazekas, F., Chawluk, J., Alavi, A., Hurtig, H., & Zimmerman, R. (1987). MR signal abnormalities at 1.5 T in Alzheimer's dementia and normal aging.

- American Journal of Roentgenology*, 149, 351–356. <http://www.ajronline.org/doi/10.2214/ajr.149.2.351>
- Forman, S. D., Cohen, J. D., Fitzgerald, M., Eddy, W. F., Mintun, M. A., & Noll, D. C. (1995). Improved assessment of significant activation in functional magnetic resonance imaging (fMRI): Use of a cluster-size threshold. *Magnetic Resonance in Medicine*, 33, 636–647. http://www.ncbi.nlm.nih.gov/entrez/query.fcgi?cmd=Retrieve&db=PubMed&dopt=Citation&list_uids=7596267
- Gao, Y.-Z., Zhang, J.-J., Liu, H., Wu, G.-Y., Xiong, L., & Shu, M. (2013). Regional cerebral blood flow and cerebrovascular reactivity in Alzheimer's disease and vascular dementia assessed by arterial spin labeling magnetic resonance imaging. *Current Neurovascular Research*, 10, 49–53. <http://openurl.ingenta.com/content/xref?genre=article&issn=1567-2026&volume=10&issue=1&spage=49>
- Gardumi, A., Ivanov, D., Havlicek, M., Formisano, E., & Uludağ, K. (2017). Tonotopic maps in human auditory cortex using arterial spin labeling. *Human Brain Mapping*, 38, 1140–1154.
- Gates, G. A., Gibbons, L. E., McCusry, S. M., Crane, P. K., Feeney, M. P., & Larson, E. B. (2010). Executive dysfunction and presbycusis in older persons with and without memory loss and dementia. *Cognitive and Behavioral Neurology*, 23, 218–223. [https://doi.org/10.1016/S1672-2930\(10\)50016-3](https://doi.org/10.1016/S1672-2930(10)50016-3) <https://doi.org/10.1038/ejhg.2014.56> http://link.springer.com/chapter/10.1007/978-0-387-72561-1_6 <http://www.ncbi.nlm.nih.gov/pubmed/17875861> <http://search.ebscohost.com/login.aspx?direct=true>
- Goebel, R., Esposito, F., & Formisano, E. (2006). Analysis of functional image analysis contest (FIAC) data with brainvoyager QX: From single-subject to cortically aligned group general linear model analysis and self-organizing group independent component analysis. *Human Brain Mapping*, 27, 392–401. <http://doi.wiley.com/10.1002/hbm.20249>
- Golub, J. S. (2017). Brain changes associated with age-related hearing loss. *Current Opinion in Otolaryngology & Head and Neck Surgery*, 25, 347–352. <http://insights.ovid.com/crossref?an=00020840-900000000-99333>
- Huang, Q., & Tang, J. (2010). Age-related hearing loss or presbycusis. *European Archives of Oto-Rhino-Laryngology*, 267, 1179–1191.
- Husain, F. T., Medina, R. E., Davis, C. W., Szymko-bennett, Y., Simonyan, K., Pajor, N. M., & Horwitz, B. (2011). Neuroanatomical changes due to hearing loss and chronic tinnitus: A combined VBM and DTI study. *Brain Research*, 1369, 74–88.
- Iadecola, C. (2017). The neurovascular unit coming of age: A journey through neurovascular coupling in health and disease. *Neuron*, 96, 17–42. <https://linkinghub.elsevier.com/retrieve/pii/S0896627317306529>
- Irvine, D., & Rajan, R. (1996). Sensory cortex of adult mammals: Possible relationship to perceptual learning. *Clinical and Experimental Pharmacology & Physiology*, 23, 939–947.
- Johnston, M. E., Lu, K., Maldjian, J. A., & Jung, Y. (2015). Multi-TI arterial spin labeling MRI with variable TR and bolus duration for cerebral blood flow and arterial transit time mapping. *IEEE Transactions on Medical Imaging*, 34, 1392–1402. <http://ieeexplore.ieee.org/document/7017519/>
- Kidd, A. R., III, & Bao, J. (2012). Recent advances in the study of age-related hearing loss: A mini-review. *Gerontology*, 58, 490–496. <http://www.karger.com/doi/10.1159/000338588>
- Kim, J.-J., Crespo-Facorro, B., Andreasen, N. C., O'Leary, D. S., Zhang, B., Harris, G., & Magnotta, V. A. (2000). An MRI-based parcellation method for the temporal lobe. *NeuroImage*, 11, 271–288. <http://linkinghub.elsevier.com/retrieve/pii/S1053811900905433>
- König, O., Schaette, R., Kempter, R., & Gross, M. (2006). Course of hearing loss and occurrence of tinnitus. *Hearing Research*, 221, 59–64.
- Kramme, J., Gregori, J., Diehl, V., Madai, V. I., von Samson-Himmelstjerna, F. C., Lentschig, M., ... Günther, M. (2015). Improving perfusion quantification in arterial spin labeling for delayed arrival times by using optimized acquisition schemes. *Zeitschrift für Medizinische Physik*, 25, 221–229. <https://doi.org/10.1016/j.zemedi.2014.07.003>
- Kurabi, A., Keithley, E. M., Housley, G. D., Ryan, A. F., & Wong, A. C. Y. (2017). Cellular mechanisms of noise-induced hearing loss. *Hearing Research*, 349, 129–137. <https://doi.org/10.1016/j.heares.2016.11.013>
- Langers, D. R. M., van Dijk, P., Schoenmaker, E. S., & Backes, W. H. (2007). fMRI activation in relation to sound intensity and loudness. *NeuroImage*, 35, 709–718. <http://linkinghub.elsevier.com/retrieve/pii/S1053811906012031>
- Lee, K.-Y. (2013). Pathophysiology of age-related hearing loss (peripheral and central). *Korean Journal of Audiology*, 17, 45–49.
- Lin, F. R., Ferrucci, L., An, Y., Goh, J. O., Doshi, J., Metter, E. J., ... Resnick, S. M. (2014). Association of hearing impairment with brain volume changes in older adults. *NeuroImage*, 90, 84–92.
- Lin, F. R., Thorpe, R., Gordon-Salant, S., & Ferrucci, L. (2011). Hearing loss prevalence and risk factors among older adults in the United States. *The Journals of Gerontology. Series A, Biological Sciences and Medical Sciences*, 66A, 582–590. <https://academic.oup.com/biomedgerontology/article-lookup/doi/10.1093/gerona/glr002>
- Liu, Y., Zeng, X., Wang, Z., Zhang, N., Fan, D., & Yuan, H. (2015). Different post label delay cerebral blood flow measurements in patients with Alzheimer's disease using 3D arterial spin labeling. *Magnetic Resonance Imaging*, 33, 1019–1025. <https://doi.org/10.1016/j.mri.2015.05.001>
- Madhyastha, T. M., Askren, M. K., Boord, P., Zhang, J., Leverenz, J. B., & Grabowski, T. J. (2015). Cerebral perfusion and cortical thickness indicate cortical involvement in mild Parkinson's disease. *Movement Disorders*, 30, 1893–1900.
- Mazelová, J., Popelar, J., & Syka, J. (2003). Auditory function in presbycusis: Peripheral vs. central changes. *Experimental Gerontology*, 38, 87–94.
- Mutsaerts, H. J. M. M., van Dalen, J. W., Heijtel, D. F. R., Groot, P. F. C., Majoie, C. B. L. M., Petersen, E. T., ... Nederveen, A. J. (2015). Cerebral perfusion measurements in elderly with hypertension using arterial spin labeling. *PLoS One*, 10, e0133717. <http://dx.plos.org/10.1371/journal.pone.0133717>
- Nasreddine, Z. S., Phillips, N. A., Bédirian, V., Charbonneau, S., Whitehead, V., Collin, I., ... Chertkow, H. (2005). The Montreal Cognitive Assessment, MoCA: A brief screening tool for mild cognitive impairment. *Journal of the American Geriatrics Society*, 53, 695–699. <http://www.ncbi.nlm.nih.gov/pubmed/15817019>
- Rajan, R., Irvine, D. R. F., Wise, L. Z., & Heil, P. (1993). Effect of unilateral partial cochlear lesions in adult cats on the representation of lesioned and unlesioned cochleas in primary auditory cortex. *The Journal of Comparative Neurology*, 338, 17–49.
- Schecklmann, M., Vielsmeier, V., Steffens, T., Landgrebe, M., Langguth, B., & Kleinjung, T. (2012). Relationship between audiometric slope and tinnitus pitch in tinnitus patients: Insights into the mechanisms of tinnitus generation. *PLoS One*, 7, e34878.
- Schonwiesner, M., Rübsem, R., & Von Cramon, D. Y. (2005). Hemispheric asymmetry for spectral and temporal processing in the human antero-lateral auditory belt cortex. *The European Journal of Neuroscience*, 22, 1521–1528.
- Schuknecht, H. F., & Gacek, M. R. (1993). Cochlear pathology in presbycusis. *The Annals of Otolaryngology, Rhinology, and Laryngology*, 102, 8420477.
- Seifritz, E., Di Salle, F., Esposito, F., Herdener, M., Neuhoff, J. G., & Scheffler, K. (2006). Enhancing BOLD response in the auditory system by neurophysiologically tuned fMRI sequence. *NeuroImage*, 29, 1013–1022.
- Sininger, Y. S., & De Bode, S. (2008). Asymmetry of temporal processing in listeners with normal hearing and unilaterally deaf subjects. *Ear and Hearing*, 29, 228–238.
- Telischak, N. A., Detre, J. A., & Zaharchuk, G. (2015). Arterial spin labeling MRI: Clinical applications in the brain. *Journal of Magnetic Resonance Imaging*, 41, 1165–1180. <http://doi.wiley.com/10.1002/jmri.24751> <http://www.ncbi.nlm.nih.gov/pubmed/25236477>
- Tzourio-Mazoyer, N., Landeau, B., Papathanassiou, D., Crivello, F., Etard, O., Delcroix, N., ... Joliot, M. (2002). Automated anatomical labeling of activations in SPM using a macroscopic anatomical parcellation of the MNI MRI single-subject brain. *NeuroImage*, 15, 273–289.
- Vemuri, P., Lesnick, T. G., Przybelski, S. A., Graff-Radford, J., Reid, R. I., Lowe, V. J., ... Jack, C. R. (2018). Development of a cerebrovascular magnetic resonance imaging biomarker for cognitive aging. *Annals of Neurology*, 84, 705–716. <http://doi.wiley.com/10.1002/ana.25346>
- Verfaillie, S. C. J., Adriaanse, S. M., Binnewijzend, M. A. A., Benedictus, M. R., Ossenkoppele, R., Wattjes, M. P., ... Barkhof, F. (2015). Cerebral perfusion and glucose metabolism in Alzheimer's disease and frontotemporal dementia: Two sides of the same coin? *European Radiology*, 25, 3050–3059. <http://link.springer.com/10.1007/s00330-015-3696-1>
- Verger, A., Roman, S., Chaudat, R. M., Felician, O., Ceccaldi, M., Didic, M., & Guedj, E. (2017). Changes of metabolism and functional connectivity in late-onset deafness: Evidence from cerebral18F-FDG-PET. *Hearing Research*, 353, 8–16.

- Vidorreta, M., Wang, Z., Rodríguez, I., Pastor, M. A., Detre, J. A., & Fernández-Seara, M. A. (2013). Comparison of 2D and 3D single-shot ASL perfusion fMRI sequences. *NeuroImage*, *66*, 662–671. <http://linkinghub.elsevier.com/retrieve/pii/S1053811912010919>
- Wolak, T., Cieśla, K., Lorens, A., Kochanek, K., Rusiniak, M., Pluta, A., & Wójcik, J. (2017). Tonotopic organisation of the auditory cortex in sloping sensorineural hearing loss. *Hearing Research*, *355*, 81–96. <https://doi.org/10.1016/j.heares.2017.09.012>
- Wu, W.-C., Fernández-Seara, M., Detre, J. A., Wehrli, F. W., & Wang, J. (2007). A theoretical and experimental investigation of the tagging efficiency of pseudocontinuous arterial spin. *Magnetic Resonance in Medicine*, *58*, 1020–1027.
- Zatorre, R. J., Belin, P., & Penhune, V. B. (2002). Structure and function of auditory cortex: Music and speech. *Trends in Cognitive Sciences*, *6*, 37–46.
- Zhang, Y. T., Geng, Z. J., Zhang, Q., Li, W., & Zhang, J. (2006). Auditory cortical responses evoked by pure tones in healthy and sensorineural hearing loss subjects: Functional MRI and magnetoencephalography. *Chinese Medical Journal*, *119*, 1548–1554.
- Zhao, M. Y., Mezue, M., Segerdahl, A. R., Okell, T. W., Tracey, I., Xiao, Y., & Chappell, M. A. (2017). A systematic study of the sensitivity of partial volume correction methods for the quantification of perfusion from pseudo-continuous arterial spin labeling MRI. *NeuroImage*, *162*, 384–397.

SUPPORTING INFORMATION

Additional supporting information may be found online in the Supporting Information section at the end of the article.

How to cite this article: Ponticorvo S, Manara R, Pfeuffer J, et al. Cortical pattern of reduced perfusion in hearing loss revealed by ASL-MRI. *Hum Brain Mapp*. 2019;40:2475–2487. <https://doi.org/10.1002/hbm.24538>